

Formation of nanograined structure and decomposition of supersaturated solid solution during high pressure torsion of Al–Zn and Al–Mg alloys

B.B. Straumal^{a,b}, B. Baretzky^{a,*}, A.A. Mazilkin^b, F. Phillipp^a, O.A. Kogtenkova^b,
M.N. Volkov^b, R.Z. Valiev^c

^a Max-Planck-Institut fuer Metallforschung, Heisenbergstrasse 3, D-70569 Stuttgart, Germany

^b Institute of Solid State Physics, Russian Academy of Sciences, Chernogolovka, Moscow District 142432, Russia

^c Institute for Physics of Advanced Materials, Ufa State Aviation Technical University, 450000 Ufa, Russia

Received 22 February 2004; received in revised form 1 June 2004; accepted 3 June 2004

Available online 6 July 2004

Abstract

Structure and phase composition of five binary Al–Zn and Al–Mg alloys were studied before and after high pressure torsion (HPT) with a shear strain 300. The grain size of (Al) solid solution and crystals of reinforcing second phases decreases drastically after HPT reaching nanometer range. As a result of HPT, the Zn-rich (Al) supersaturated solid solution decomposes completely and reaches the equilibrium state corresponding to room temperature. The decomposition is less pronounced for Al–Mg alloys. We conclude that the severe plastic deformation of supersaturated solid solutions can be considered as a balance between deformation-induced disordering and deformation-accelerated diffusion towards the equilibrium state.

© 2004 Acta Materialia Inc. Published by Elsevier Ltd. All rights reserved.

Keywords: High pressure torsion; Nanocrystalline materials; Enhanced diffusion

1. Introduction

One of the important ways to improve the mechanical properties is to produce materials with a very small grain size. In such materials a significant fraction of the atoms are located at the grain boundaries [1]. Among the techniques capable to produce such nanostructured materials, a certain number (e.g. inert gas condensation, ball-milling) result in the production of powders which must be subsequently consolidated. In contrast, methods based on severe plastic deformation (SPD) can produce nanomaterials which are large in size and have full density. In contrast to the conventional processes of high deformation like rolling or wire drawing, which strongly change the geometry of the sample, SPD techniques namely, equal channel angular pressing (ECAP) and high pressure torsion (HPT), do not involve changes in the material

geometry, but they lead to strong grain refinement [2,3]. The possibility of producing bulk metals with a grain size in submicrometer and nanometer ranges using these methods have been demonstrated up to date for many metallic materials [4]. It has been also shown that SPD of pure metals and multiphase alloys allows obtaining materials with ultrafine grains or a phase composition that is impossible to be produced by conventional thermal treatment. One can mention for example the formation of supersaturated solid solutions in immiscible Al–Fe alloys and pearlitic steel [5–8], disordering or even amorphization of intermetallics during the SPD [9–11]. However, one important and still not clarified issue is the role of the diffusion-controlled processes during SPD. In the conventional thermo-mechanical treatment a clear difference exists between cold work and deformation at elevated temperature. At high temperatures the diffusion fluxes are high and ensure the recovery processes which proceed simultaneously with deformation at a comparable rate. During conventional cold work the diffusion can be

* Corresponding author. Fax: +49-71-16-89-3412.

E-mail address: baretzky@mf.mpg.de (B. Baretzky).

neglected and the resulting microstructure and properties of a material are completely controlled by the deformation. Heavy plastic deformation produces many lattice defects, and one can suppose that the vacancy and/or interstitial production during the SPD are high enough to allow diffusion-controlled recovery. Such recovery proceeds simultaneously with the deformation even at low temperature. It is well known, that vacancies produced during irradiation can induce the diffusion fluxes and allow to reach the thermodynamically equilibrium phase structure at low temperatures (e.g. by decomposition of solid solution or formation of low-temperature phases) [12]. Therefore, one can assume that under some conditions SPD can simultaneously lead to the refinement of the grain structure (the path leading away from the equilibrium) and to release the kinetically suppressed processes of formation of phases which are in equilibrium at temperature and pressure of the SPD treatment (the path leading towards the equilibrium).

In order to clarify this issue we have chosen two binary Al-based systems, namely Al–Mg and Al–Zn. First of all, these systems are the base for numerous industrial alloys. The diffusivity of Zn in the Al matrix is much higher than that of Mg [13–15]. The addition of Zn decreases and that of Mg increases the lattice spacing of Al [16–18]. In Al–Zn alloys the matrix is strengthened by metallic Zn precipitates [19]. In Al–Mg alloys the precipitates are the intermetallic compounds [19,20]. Data on the influence of pressure and irradiation for these systems may be found elsewhere [21–24]. The processes during HPT can be substantially influenced by the formation of layers of grain boundaries (GB) phases which are stable in GBs and unstable in the bulk [25–27]. Such phases form as a result of wetting, premelting and prewetting GB phase transitions [25–30]. GB phases can strongly affect the GB energy [31], GB segregation [25,31,32], diffusion [28,29,33–36], mechanical [25,32] and electrical [37] properties of polycrystals. The GB wetting phase transitions were recently observed in Al–Mg and Al–Zn systems [38,39]. If the tie-lines of GB wetting phase transitions exist in the two-phase solid + liquid region of the bulk phase diagram, these tie-lines have to continue into the one-phase solid solution region of the bulk Al–Mg and Al–Zn alloys as GB solidus lines. The hypothesis was proposed that the high strain rate superplasticity observed in ternary Al–Mg–Zn alloys [40,41] proceeds between the GB and bulk solidus lines and is driven by the formation of specific GB phases in these alloys [38,39,42].

2. Experimental

Five binary Al-based alloys (with 10, 20 and 30 wt% Zn, with 5 and 10 wt% Mg) were prepared by vacuum induction melting and casting into 9 mm diameter rods.

They were made of high purity components (5N5 Al, 5N Zn of and 4N5 Mg). As-cast disks of these alloys with thickness of 0.3 mm and with a coarse-grained (CG) structure were prepared from the rods by grinding, spark erosion, sawing and chemical etching in 47% HCl + 50% HNO₃ + 3% H₂O solution. The as-cast alloys were subjected to SPD by torsion at room temperature under the pressure of 5 GPa in a Bridgman anvil type unit (5 torsions, duration of process about 300 s) [4]. The sample was placed between an upper immobile and lower rotatable Bridgman anvil. Due to the high thermoconductivity of anvils and good thermal contact the temperature of the sample during HPT remains below 50 °C. Torsion straining of a disc sample of diameter $2R$ and thickness h produces a shear strain γ which varies from zero on the sample axis to a maximum value γ_{\max} on the lateral surface (situated at a distance R from the axis):

$$\gamma_{\max} = 2\pi nr/h, \quad (1)$$

n being the number of rotations of the mobile anvil, r being the distance from the sample centre. For comparison of shear deformation with tensile strain, the equivalent strain value e_{eq} can be used [43,44]:

$$e_{\text{eq}} = \gamma/\sqrt{3} = 2\pi nR/h\sqrt{3}. \quad (2)$$

All samples for the investigations were cut from the deformed disks at a distance of 5 mm from the sample centre. For this distance the shear strain γ is 520 and the equivalent strain value e_{eq} is 300. This strain value has been typically used for the production of nanomaterials in earlier studies [2–4,11,43–45].

Transmission electron microscopy (TEM) investigations have been carried out on a JEM-4000FX microscope at an accelerating voltage of 400 kV. The microscope is equipped with a Gresham energy dispersive X-ray (EDX) microanalysis system with a high-purity Ge detector. It was used for the local analysis of the alloying element concentration. Samples for the TEM investigations were prepared by the jet electropolishing technique in a 75% methanol + 25% nitric acid solution at a temperature –30 °C. The phase constitution of the alloys was analysed by selected area electron diffraction. Dislocation density in TEM investigations was measured using a conventional technique by counting the number of dislocation intersections with a line of a definite length. X-ray diffraction (XRD) data were obtained on a SIEMENS-500 diffractometer with a graphite monochromator and line position sensitive gas flow detector. Cu K_{α1} radiation was used. To obtain the lattice parameters of the studied alloys reflections in a high-angle interval ($2\theta > 100^\circ$) were taken into account. The precise centroid position of the profile was determined by an approximation procedure with a Lorentz function. Lattice parameters were determined by the Nelson–Riley extrapolation technique [46,47]; the

relative error was about 0.01%. The XRD profile treatment known as improved Williamson–Hall procedure [4,49] was applied to obtain values of the mean grain size in the Al–Mg alloys after the HPT deformation.

3. Results

Fig. 1 represents the microstructure of the CG Al–30 wt% Zn alloy (state before HPT deformation). The alloy contains isolated grains of (Zn) solid solution among the grains of (Al) solid solution. Both (Al) and (Zn) grains are almost dislocation-free with a dislocation density about 10^{10} m^{-2} . The dislocations are distributed uniformly. The mean grain size in all studied Al–Zn alloys is about $500 \mu\text{m}$ for (Al) and $3\text{--}5 \mu\text{m}$ for (Zn). The XRD data have also revealed the presence of (Al) and (Zn) phases. The microstructures of the Al–10 wt% Zn and Al–20 wt% Zn alloys are similar to that of the Al–30 wt% Zn alloy but contains lower amount of (Zn) phase. The grains of (Al) phase are large enough to measure the Zn concentration by EDX. Zn concentration was also estimated based on the values of lattice spacing measured by XRD and on the published data of lattice spacing in Al–Zn solid solutions [16]. Respective values are shown in Fig. 2. They are nearly equal to the solidus concentrations at temperatures of 340, 460 and 480 K, correspondingly. It means that in CG alloys the (Al) solid solution is supersaturated at room temperature (i.e. temperature of the following HPT deformation).

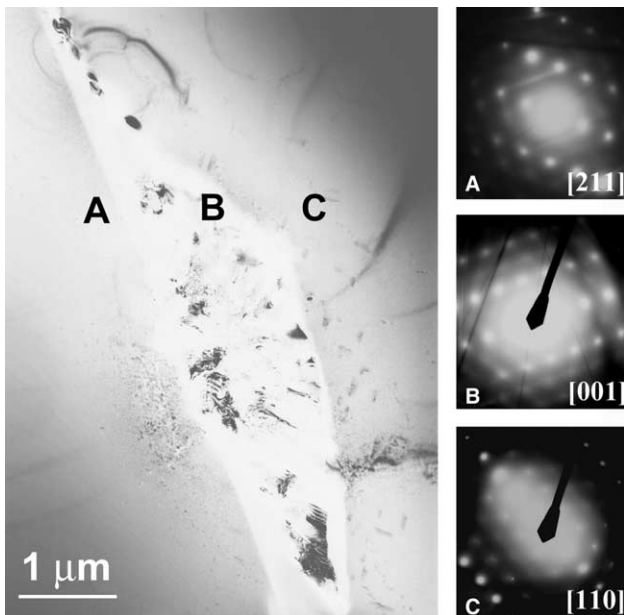


Fig. 1. Microstructure of the CG Al–30 wt% Zn alloy (state before HPT deformation). Bright field TEM micrograph showing a (Zn) grain (B) at the GB between two (Al) grains (A and C) with respective electron diffraction patterns.

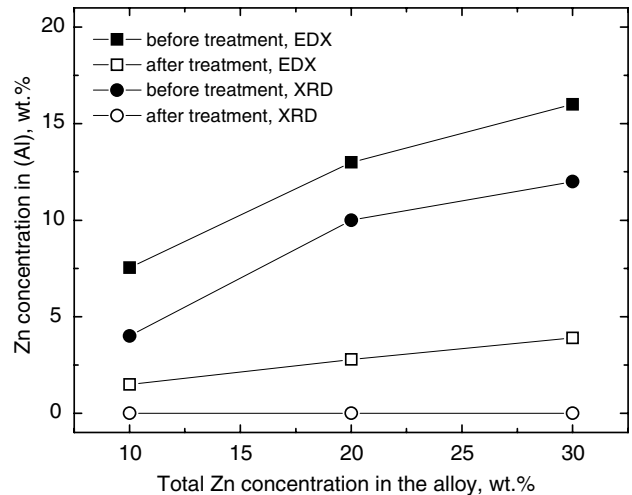


Fig. 2. Concentration of Zn in (Al) solid solutions in various Al–Zn alloys before and after HPT.

Fig. 3 represents the microstructure of the CG Al–10 wt% Mg alloy (state before HPT deformation). The alloy contains grains of (Al) solid solution with a mean size of $500 \mu\text{m}$. The dislocation density in (Al) is about 10^{12} m^{-2} and is, therefore, higher than that of Al–Zn alloys. The dislocations are distributed non-uniformly and subgrain boundaries are visible (points A, B, C in Fig. 3(a)). Microdiffraction reveals the presence of β -phase Al_3Mg_2 . The fine Al_3Mg_2 particles have size about 10 nm (dark field image in Fig. 2(b)). They form fine-crystalline colonies with a mean size of about $2\text{--}3 \mu\text{m}$. The microdiffraction pattern obtained from such a colony contains both Al and Al_3Mg_2 reflections (Fig. 3(b)). Absence of characteristic rings demonstrates that the Al_3Mg_2 particles are specially oriented and are probably coherent with the (Al) matrix. Microstructure of the Al–5 wt% Mg alloy is similar to that of the Al–10 wt% Mg alloy, containing lower amount of β -phase. The data of XRD do not reveal the presence of Al_3Mg_2 phase, which means that its fraction is less than 1 vol%. Mean Mg concentrations in (Al) for Al–5 wt% Mg and Al–10 wt% Mg CG alloys measured by XRD using the reference data for Al–Mg solid solutions [50,51] are 2.8 and 3.9 wt% Mg correspondingly. The EDX measurements yield 3.0 and 4.9 wt% Mg. The obtained Mg concentrations are equal to the solidus concentrations in alloys at temperatures of 450 and 570 K, correspondingly. Therefore, in CG alloys the (Al) solid solution at room temperature (temperature of the following HPT deformation) is in the supersaturated state.

Specimens of all studied Al–Zn alloys after HPT have two phases, and two kinds of grains are observed in the structure (Fig. 4). These are (Al) grains with a size of $\sim 800 \text{ nm}$ (instead of $500 \mu\text{m}$ before HPT) and grains of (Zn) which size is about $\sim 200 \text{ nm}$ (instead of $3\text{--}5 \mu\text{m}$ before HPT). The dislocation density for these alloys is

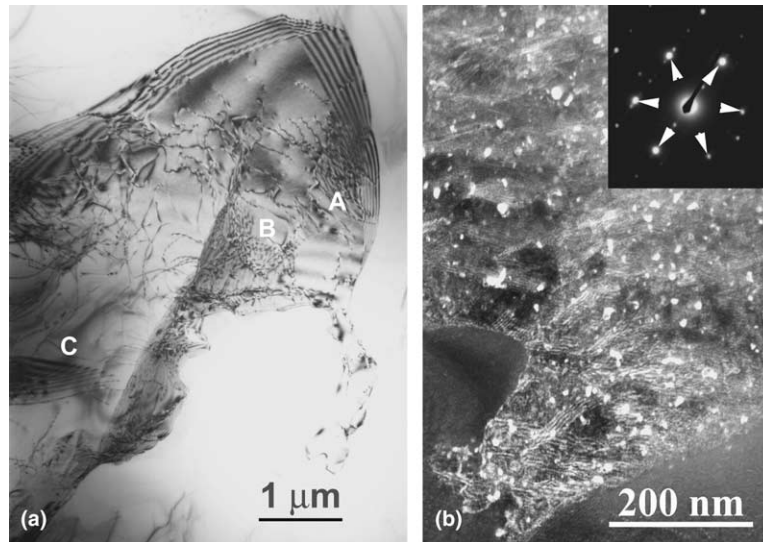


Fig. 3. Microstructure of the CG Al-10 wt% Mg alloy (state before HPT deformation). (a) bright field micrograph (A, B and C – subgrain boundaries). (b) Dark field image of a colony of β -phase particles. The microdiffraction pattern with reflections for the β -phase and (Al) is shown in the insert. (Al) reflections are indicated by arrows.

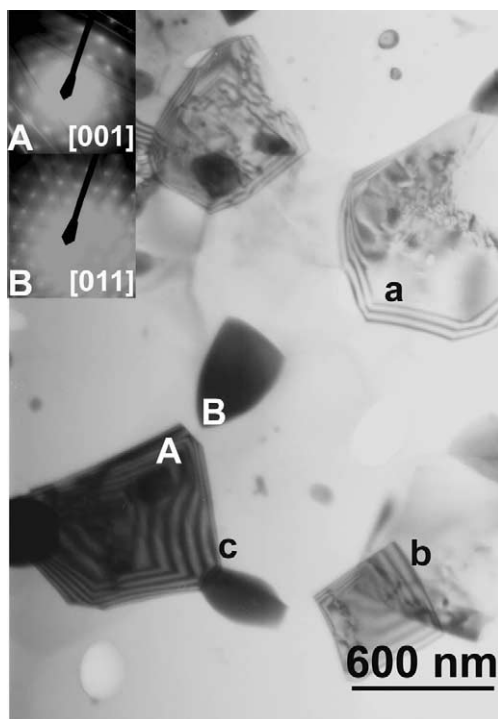


Fig. 4. Microstructure of the Al-20 wt% Zn alloy after HPT deformation. Bright field TEM micrograph showing (Al) and (Zn) grains with extinction contours in points a, b and c. Electron diffraction patterns for (Al) and (Zn) grains are also shown in points A and B correspondingly.

rather low and is about 10^{12} m^{-2} . It is only slightly higher than in the CG alloys. The grains are practically equiaxial with distinct extinction contours (points a, b and c in Fig. 4(a)). The microstructure of all studied Al-Zn alloys after HPT is similar. XRD and EDX data

on Zn concentration in solid solution are presented in Fig. 2. The Zn content in (Al) decreased after HPT and almost corresponds to the equilibrium solubility at room temperature. Fig. 5 displays the data on grain size of (Al) solid solution and second phases, (Zn) and Al_3Mg_2 , before and after HPT deformation.

Fig. 6 represents the structure of the Al-5 wt% Mg alloy after the HPT deformation. Grains with a size of about 150 nm (instead of 500 μm before HPT) are detected in the structure (Fig. 6(a) and (c)). Dislocation density is very high ($>10^{14} \text{ m}^{-2}$ which is the limit for the determination by conventional TEM). It is considerably higher as compared to Al-Zn alloys. Dislocations are observed to be mainly arranged in subgrain boundaries (Fig. 6(a), points A and B). Selected area diffraction

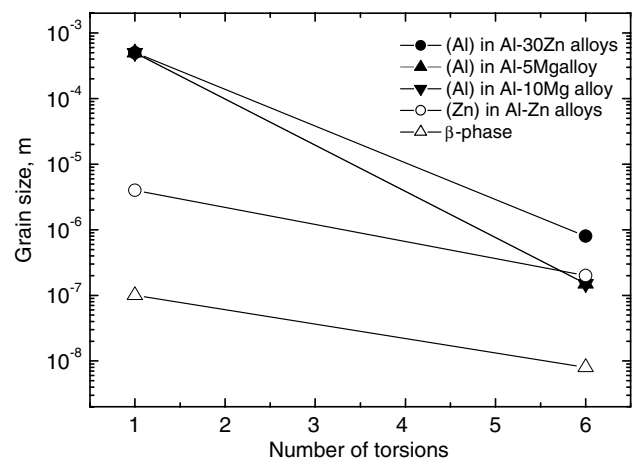


Fig. 5. Grain size of (Al) solid solution and second phases (Zn) and Al_3Mg_2 before and after HPT.

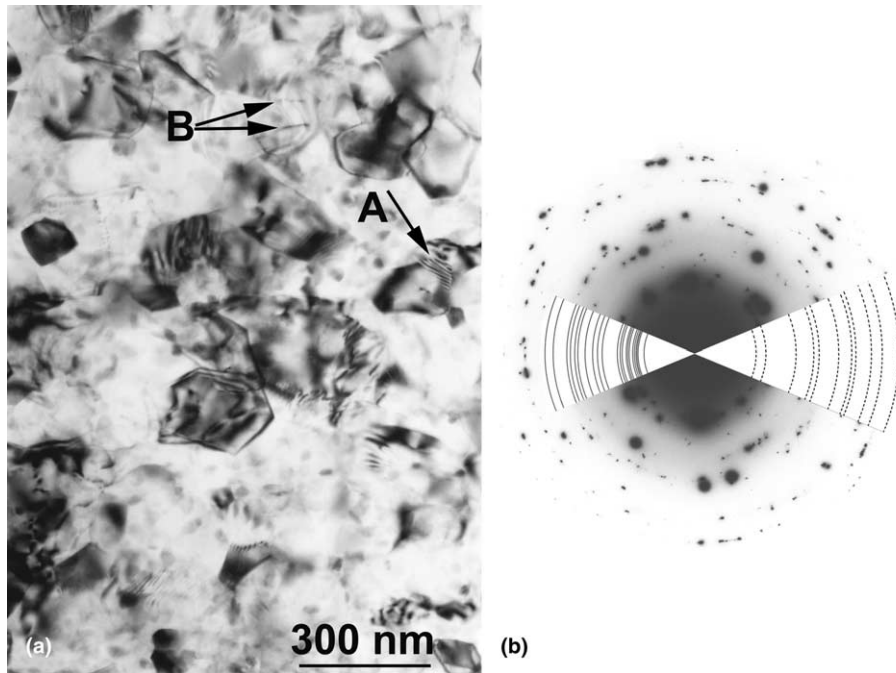


Fig. 6. Microstructure of the Al-5 wt% Mg alloy after HPT deformation. (a) Bright field (BF) micrograph. A – Dislocations. B – subgrain boundaries. (b) SAED with reflexes of Al (solid lines) and β -phase (dotted lines). The positions of rings are also shown for β -phase (left) and Al (right). β -phase reflections (771), (17 5 3); (11 1 1), (14 12 4); (880), (14 14 0); (882), (21 3 1); (11 3 3), (16 16 0); (11 5 1), (23 3 1); (12 4 2), (17 17 1); (10 6 6), (20 14 4); (13 3 1), (26 6 6); (10 10 0), (23 15 1); (11 9 3), (24 16 2); (15 1 1), (29 1 1); Al reflections (1 1 1), (2 0 0), (2 2 0), (3 1 1), (2 2 2), (4 0 0), (3 3 1), (4 2 0), (4 2 2), (5 1 1), (5 3 1).

(SAED) patterns revealed the presence of the β -phase (Al_3Mg_2) particles (Fig. 6(b)). They are uniformly distributed in the material. The particles of the β -phase are extremely dispersed. Therefore, they cannot be distinguished in the conventional TEM micrographs and they were detected by the additional spots in the electron diffraction pattern (Fig. 6(b)). X-ray analysis did not detect the β -phase in the alloy. It implies that its volume fraction is not higher than 1%. The grain size of β -phase can be estimated as <10 nm. The alloy with 10% of Mg has similar structure with a smaller (Al) grain size of about 90 nm. It was impossible to measure the Mg concentration in (Al) by EDX since β -particles are very fine, randomly distributed and cannot be excluded from the analysing field. XRD data yield values 2.1 wt% Mg and 4.1 wt% Mg for Al-5 wt% Mg and Al-10 wt% Mg alloys, respectively.

It is known that both small grain size (less than 500 nm) and internal stress contribute to X-ray line broadening. The method to separate these contributions is known as Williamson–Hall procedure [52]. The procedure was modified by Ungar et al. [53,54]. Assuming that the stress broadening is caused by dislocations, the full width at half maximum (FWHM) $\Delta(2\theta)$ of the line profile can be determined from the equation for $\Delta K = \cos\theta[\Delta(2\theta)]/\lambda$:

$$\Delta K = \gamma/D + \alpha(KC^{1/2}) + O(K^2C), \quad (3)$$

where K is the length of the diffraction vector, θ is the diffraction angle, λ is X-ray wave length, D is a size parameter, γ equals to 0.9, α is a constant depending on the effective outer cut-off radius, the Burgers vector and the density of dislocations, C is the contrast factor of dislocations, ‘ O ’ stands for higher order terms in $KC^{1/2}$. The slope of ΔK vs. $KC^{1/2}$ plot yields the dislocation density. According to Eq. (3) the size parameter is obtained by extrapolation to $\Delta K = 0$.

We investigated the angular dependence of the FWHM in Al–Mg alloys. In Fig. 7 the modified

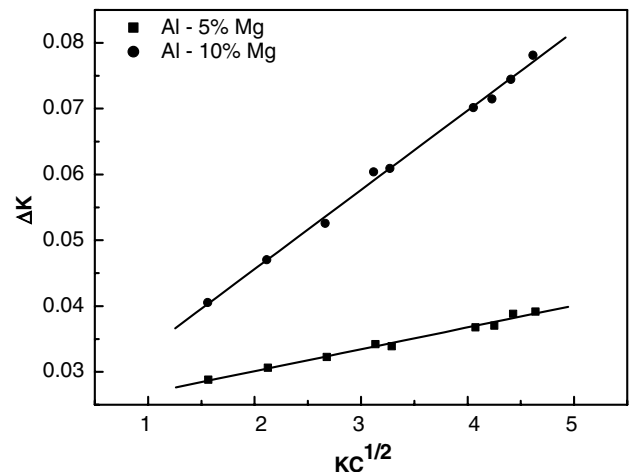


Fig. 7. Modified Williamson–Hall plots for Al–Mg alloys.

Williamson–Hall plot is presented. The dislocation contrast factor C was calculated after [55]. The FWHM of the profiles was determined taking into account the instrumental broadening. For Al–Mg alloys the size of the crystallites is 39 nm and 41 nm and the dislocation density $\rho = 6.2 \times 10^{15}$ and $1.3 \times 10^{16} \text{ m}^{-2}$ for the alloys with 5% and 10% Mg, correspondingly. From this plot

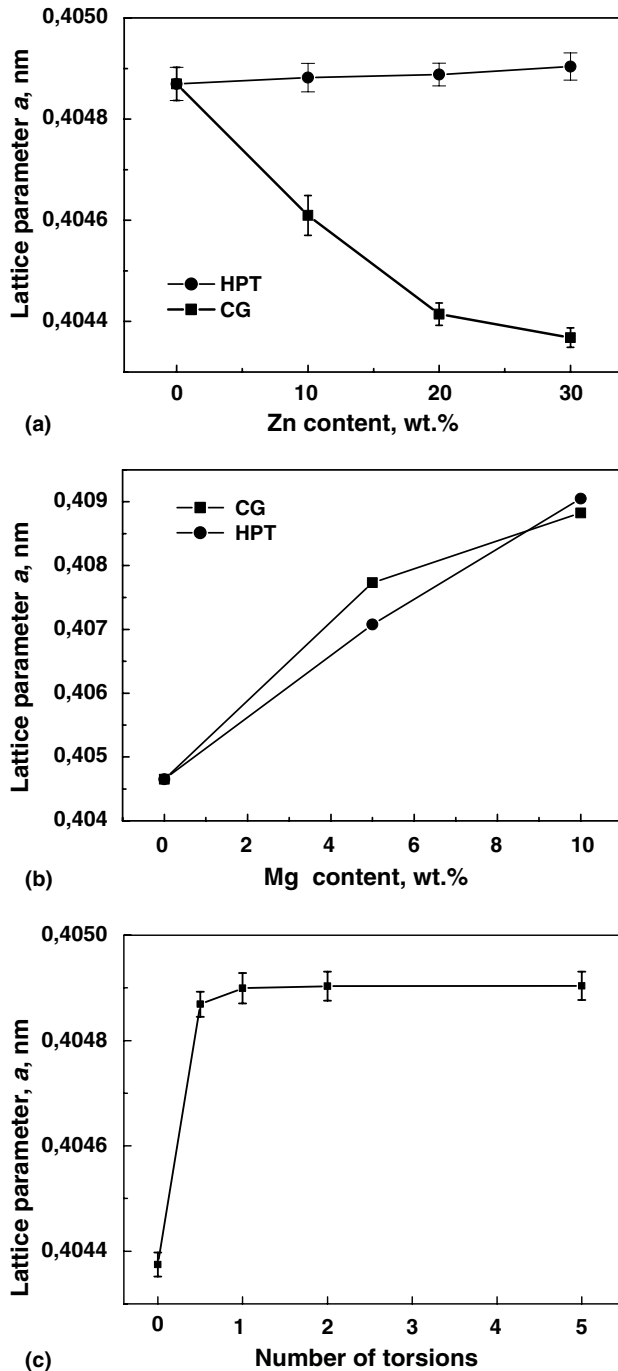


Fig. 8. Dependence of the lattice parameter vs. the alloying element concentration in (a) Al–Zn and (b) Al–Mg alloys. (c) Dependence of the lattice parameter vs. the deformation degree in the Al–30 wt% Zn alloy.

one can see that increased Mg concentration leads also to a higher dislocation density and work hardening. The values of grain size obtained from TEM studies and from XRD analysis are slightly different. It can be explained by the presence of subboundaries in the alloy structure. X-ray data yield most probably the size of the subgrains or dislocation cells [48].

For two investigated systems the dependence of the lattice parameter vs. the alloying element concentration was obtained for both CG and HPT-deformed specimens (Fig. 8). It can be seen from Fig. 8(a) for Al–Zn alloys that the lattice parameter a increases after HPT deformation, therefore, recovering to the values close to that of pure Al. It means that the phase state of the material after HPT deformation is closer to the equilibrium than that for CG material. Fig. 8(c) demonstrates that the lattice parameter a in the Al–30 wt% Zn alloy increases very fast during HPT. The value of a already reaches its final value y after one torsion (Fig. 8(c)). In Al–Mg alloys the lattice parameter decreases after HPT deformation. However, in Al–Mg alloys such recovery is much less pronounced.

4. Discussion

4.1. Grain refinement and equilibration of phases during high pressure torsion

According to the equilibrium phase diagrams the Al–10 wt% Zn, Al–20 wt% Zn and Al–30 wt% Zn alloys have to contain at atmospheric pressure and room temperature the (Al) solid solution with Zn content less than 0.5 wt% and (Zn) solid solution with Al content less than 0.1 wt% [19]. In the Al–5 wt% Mg and Al–10 wt% Mg alloys (Al) solid solution with Mg content less than 1 wt% and β -phase Al_3Mg_2 has to be present [19]. Only the volume ratio of these phases is different at different Zn and Mg content. In CG samples the same phases are present, but the (Al) solid solution is in all cases supersaturated at room temperature. HPT deformation at room temperature decreases the grain size of (Al), (Zn) and β -phase (Fig. 2). It means that HPT leads from more equilibrium grain structure to less equilibrium one. On the other hand, the supersaturated (Al) solid solution decomposes in all studied samples. It means that HPT results in more equilibrium phase structure. From this point of view HPT cannot be considered as cold work, since the phase equilibration proceeds even at room temperature, similar to warm deformation at moderate strains. There is a distinct difference between the behaviour of Zn and Mg during the decomposition of supersaturated solid solution in the same HPT conditions. The Al–Zn solid solutions almost completely decompose and reach the equilibrium

concentration at room temperature. The decomposition of Al–Mg solid solutions proceeds only partly.

4.2. Bulk diffusion as a possible mechanism of recovery during HPT

The supersaturation is the driving force for the bulk diffusion of Zn and Mg from the solid solution to the sinks which are the particles of (Zn) and β -phase, respectively. The diffusion paths for individual Zn and Mg atoms would be about 800 and 100 nm, respectively. It corresponds to the bulk diffusion coefficients of $10^{-15} \text{ m}^2 \text{ s}^{-1}$ for Zn and $10^{-17} \text{ m}^2 \text{ s}^{-1}$ for Mg. There are two groups of tracer diffusion data for bulk diffusion of Zn in Al: measured in polycrystals ($D_0 = 0.30 \times 10^{-4} \text{ m}^2 \text{ s}^{-1}$, $Q = 121.4 \text{ kJ mol}^{-1}$, obtained within the range 700–920 K, ^{65}Zn , [14]) and single crystals ($D_0 = 0.259 \times 10^{-4} \text{ m}^2 \text{ s}^{-1}$, $Q = 120.8 \text{ kJ mol}^{-1}$, 630–926 K, ^{65}Zn [13]). After the extrapolation to 300 K the both data yield very close values of $D(300\text{K}) = 0.95 \times 10^{-23} \text{ m}^2 \text{ s}^{-1}$ and $D(300\text{K}) = 1.0 \times 10^{-23} \text{ m}^2 \text{ s}^{-1}$. This is about 8 orders of magnitude less than the value estimated from the diffusion path of the actual solid-solution decomposition during HPT. Extrapolation of the data for Mg bulk diffusion in Al single crystals ($D_0 = 1.24 \times 10^{-4} \text{ m}^2 \text{ s}^{-1}$, $Q = 130.4 \text{ kJ mol}^{-1}$, 667–928 K, ^{28}Mg [15]) gives $D(300\text{K}) = 1.7 \times 10^{-24} \text{ m}^2 \text{ s}^{-1}$. It means that though Mg diffuses slower than Zn, the difference of about 8 orders of magnitude remains unexplained. The question arises: can HPT produce additional vacancies for acceleration of bulk diffusion, similar to those produced by the irradiation of materials?

Early estimations of the vacancy production during cold work were made based on the data for residual resistivity measurements [56]. In metals the residual resistivity attributed to point defects increases with the strain ε according to the laws which vary somewhat with the type of the stress-strain curve. From the residual resistivity per Frenkel pair, deduced from irradiation experiments, it was concluded that atomic concentrations of 10^{-5} to 10^{-4} are reached for strains $\varepsilon \approx 1$ [57,58]. Therefore, even a strain of $\varepsilon \approx 1$ produces the vacancy concentration comparable to the equilibrium value at the melting point (about 10^{-4} [56]). The recombination of the dislocations other than screws placed in neighboring parallel planes has been considered as a most possible mechanism for the vacancy production [56]. Deformation dependence of the atomic concentration c of point defects may be written as:

$$dc/d\varepsilon = \sigma/3\mu, \quad (4)$$

(μ being the shear modulus, σ being the stress value). This law is relatively well followed in face centred cubic metals [59–61]. Within the linear deformation stage it predicts a parabolic increase of c . From $d\sigma/d\varepsilon \approx \mu/200$ it follows $c \approx 10^{-4}\varepsilon^2$. This estimation agrees well with

measurements on copper giving $c \approx 10^{-5}$ to 10^{-4} for strains $\varepsilon \approx 1$ [57,58]. Formal application of this relation for our case $\varepsilon \approx 400$ results in enormous total vacancy production during the deformation process (total concentration of 2) which is for sure enough for every equilibration. However, it is unclear, whether the dislocation mechanism for the vacancy production, proposed for low deformations, remains valid for SPD. Therefore, we have to consider the alternative mechanism of GB diffusion.

4.3. Grain boundary diffusion as a possible mechanism of recovery during HPT

In Al–Zn alloys the supersaturated solid solution with concentration of 12 wt% completely decomposes after 300 s. The mean distance between Zn particles in the nanostructured Al–30 wt% Zn alloy is about 2 μm . It means that each particle collected the Zn atoms from the surrounding area with a radius (diffusion path) of about 2 μm . This area includes several (Al) grains and many (Al) GBs. If this process would be controlled by bulk diffusion, D could be estimated as $D = (10^{-12} \text{ m}^2/300 \text{ s}) = 3 \times 10^{-15} \text{ m}^2 \text{ s}^{-1}$ which is at least 8 orders of magnitude higher than D for conventional bulk diffusion at 300 K. The transport of Zn from the (Al) matrix can be controlled by grain boundary diffusion of Zn atoms along (Al) GBs. Let us suppose that the moving GBs during HPT swept at least once each Zn atom in the bulk, and then bulk diffusion towards GB has not to be considered. In this case the path for GB diffusion would be roughly 1 μm yielding $sD\delta$ value of $1.5 \times 10^{-24} \text{ m}^3 \text{ s}^{-1}$ for a GB thickness of $\delta = 0.5 \text{ nm}$ and a segregation factor $s = 1$.

In [60] the data were obtained for ^{65}Zn tracer GB diffusion in the 99.99% purity Al polycrystal within the temperature interval 428–593 K. Three groups of GBs were defined, namely (I) high-angle GBs with high activation energy Q of GB diffusion ($sD_0\delta = 1 \times 10^{-9} \text{ m}^3 \text{ s}^{-1}$, $Q = 118 \text{ kJ mol}^{-1}$), (II) high-angle GBs with low activation energy ($sD_0\delta = 1.6 \times 10^{-11} \text{ m}^3 \text{ s}^{-1}$, $Q = 90 \text{ kJ mol}^{-1}$) and (III) low-angle GBs between subgrains ($sD_0\delta = 6 \times 10^{-14} \text{ m}^3 \text{ s}^{-1}$, $Q = 60 \text{ kJ mol}^{-1}$). Extrapolation of these data to 300 K yield, respectively, (I) $sD\delta = 3 \times 10^{-24} \text{ m}^3 \text{ s}^{-1}$, (II) $sD\delta = 2 \times 10^{-26} \text{ m}^3 \text{ s}^{-1}$, and (III) $sD\delta = 2 \times 10^{-29} \text{ m}^3 \text{ s}^{-1}$. The first value is surprisingly close to the estimation for the diffusion path needed to the equilibration of the Al–Zn supersaturated solid solution during the HPT treatment. A similar value of $sD\delta = 10^{-23} \text{ m}^3 \text{ s}^{-1}$ obtains also from [62–64].

In [65] the parameters of Zn GB diffusion were measured by electron probe microanalysis in Al bicrystals with individual tilt and twist GBs with various misorientation angles within the interval 523–613 K. The pre-exponentials $sD_0\delta$ and activation energies Q for tilt GBs lie within the intervals 2×10^{-16} – $10^{-12} \text{ m}^3 \text{ s}^{-1}$

and 40–80 kJ mol⁻¹, respectively [65]. The pre-exponentials and activation energies for twist GBs are within the intervals 10⁻¹⁵–10⁻⁹ m³ s⁻¹ and 50–130 kJ mol⁻¹, respectively [66]. The extrapolation to 300 K yields $sD\delta$ values for tilt GBs between 10⁻²⁴ and 10⁻²² m³ s⁻¹. Therefore, all tilt GB studied in [65] and some twist GBs form a family of “high-diffusivity” GBs which can build channels for the diffusion which is fast enough to equilibrate the Al–Zn solid solutions during HPT.

In [67] the parameters of Zn GB diffusion were determined in an Al–30 wt% Zn alloy using the discontinuous precipitation reaction controlled by GB diffusion. The advantage of these measurements is that they were performed at rather low temperatures of 350–500 K. Extrapolation to 300 K yields a $sD\delta$ value of 4×10^{-23} m³ s⁻¹. Therefore, the GBs in Al provide the diffusion paths for Zn which can be responsible for the decomposition of supersaturated solid solution during HPT. The ⁶⁵Zn tracer measurements obtained in the temperature interval 493–673 K demonstrate that the increase of the Zn content can further enhance the GB diffusivity in Al–Zn alloys [68–70]. The extrapolation to 300 K yields $sD\delta$ values of 3×10^{-22} m³ s⁻¹ (2 wt% Zn), 10^{-21} m³ s⁻¹ (4.33 wt% Zn) and 10^{-20} m³ s⁻¹ (8–10 at.% Zn).

Data on Mg GB diffusion in Al are not so numerous, maybe due to the lower values of $sD\delta$. Values of $sD_0\delta = 7 \times 10^{-14}$ m³ s⁻¹ and $Q = 87$ kJ mol⁻¹ were obtained in [71,72]. The extrapolation to 300 K yields $sD\delta$ value of 5×10^{-28} m³ s⁻¹. It is about 5 orders of magnitude lower than the typical values for the Zn GB diffusivity. Direct comparison of Zn and Mg diffusion allow the data on chemical diffusion in Al–0.1 wt% Sc alloys [73]. Though the $sD\delta$ values were extracted from the comparison of integral measurements on coarse- and nanograined polycrystals obtained by ECAP (as well as in [71,72]), the data demonstrate undoubtedly a lower GB diffusivity of Mg in comparison with Zn. This fact can explain the slower decomposition of supersaturated solid solution in Al–Mg alloys studied in present work in comparison with Al–Zn alloys deformed in the same HPT conditions. Nevertheless, both Zn and Mg GB diffusivities extrapolated towards 300 K are much higher than the $sD\delta$ value for the Al GB self-diffusion (10^{-31} m³ s⁻¹ [64]). Based on (unfortunately rather scarce) data on GB diffusion in Al, one can expect that Al–Ga supersaturated solid solutions would also decompose very quickly ($sD\delta$ value extrapolated to 300 K is about 10^{-21} m³ s⁻¹ [74]).

If GB diffusion is so effective, why the supersaturated solid solution does not decompose without any HPT? The reason is in the low bulk diffusivity. The solute atoms are frozen in the bulk and cannot reach the GBs. During HPT GBs move, sweeping in such a way the “frozen” solute atoms. This mechanism is to a certain extent opposite to the well-known diffusion induced grain boundary migration (DIGM).

4.4. Influence of the high pressure and GB phase transitions

Pressure applied during the HPT was 5 GPa. It is sufficient to change the phase diagram and the diffusivity. As a result the system could evolve to the state which is in equilibrium at high pressures and differs from that at the atmospheric one. This may be analysed as follows: the solubility of Zn in (Al) decreases with increasing pressure, and no new phases appear at room temperature [21,22]. The same holds also for the Al–Mg system [23]. High pressure drastically decreases the bulk diffusivity. Minamino measured the Mg diffusivity in Al–Mg alloys at 3.3 GPa by studying the chemical diffusion in polycrystals ($D_0 = 3 \times 10^{-5}$ m² s⁻¹, $Q = 151$ kJ mol⁻¹, 667–928 K [75]). The extrapolation of these data to 300 K and 0% Mg yields $D(300\text{K}, 3.3 \text{ GPa}) = 10^{-27}$ m² s⁻¹. It is about 3 orders of magnitude lower than at atmospheric pressure (see Section 4.2). Extrapolation to 5 GPa yields $D(300 \text{ K}, 5 \text{ GPa}) = 10^{-28}$ – 10^{-29} m² s⁻¹. The data for Zn GB diffusion under high pressures in Al polycrystals [76] were obtained in conditions similar to [63]. They demonstrate that by extrapolation to 5 GPa the GB diffusivity decreases by 3.5–4.7 orders of magnitude depending on the GB class. By using the estimation made above, one obtains (I) $sD\delta = 10^{-27}$ m³ s⁻¹ and (II) $sD\delta = 10^{-30}$ m³ s⁻¹. These values are again lower than the estimated $sD\delta$ value of 1.5×10^{-24} m³ s⁻¹ needed for the equilibration of supersaturated solid solution by GB diffusion. It seems that the hypothesis of the additional vacancies produced during SPD (Section 4.2) is realistic and can explain the apparent discrepancy.

It has been shown that some GB phase transitions (prewetting, premelting) can lead to the formation of thin equilibrium layers of GB phases which are stable in the GB and unstable in the bulk [25–27]. If the grain size in matrix A decreases, the formation of GB layers consumes more and more atoms of the (second) component B. Simple geometrical considerations demonstrate that if such a layer has two monolayers of B like in the Cu–Bi system [25,31,32] it consumes about 6, 15 and 20 vol% B for a grain size $d = 50$, 20 and 10 nm, respectively. On the other hand, thin layers of GB phases do not influence significantly the XRD spectra; it is complicated to observe them in conventional TEM and even by HREM. In [8] about 2.4 vol% cementite disappeared traceless from XRD spectra and TEM micrographs by decreasing grain size to d between 50 and 20 nm. This can be explained by the formation of thin layer of a GB phase [30]. GB layers can also lead to the enhanced GB diffusivity $sD\delta$. Presence of a GB layer increases simultaneously s , D and δ values. The fact can be illustrated by the data on GB diffusivity in Fe–Si–Zn and Cu–Bi systems [28–30,33–35]. Some indications of GB phase transitions exist for Al-based systems with

high GB diffusivity like Al–Zn or Al–Ga. The data of the present work also demonstrate the difference in equilibration kinetics between Al–Zn and Al–Mg systems. Therefore, the search for the GB layers in the Al-based systems would be desirable.

5. Conclusions

1. SPD by HPT of binary Al–Zn and Al–Mg alloys decreases drastically the size of (Al) and (Zn) grains (below 100 nm) and particles of reinforcing β -phase (below 10 nm). Therefore, HPT with a shear strain of 300 leads to the formation of nanostructures which are further from the equilibrium state than the initial coarse grained material.
2. At the same time, during HPT the Zn-rich supersaturated solid solution (Al) decomposes completely and reaches the equilibrium corresponding to the room temperature. This process is less pronounced for Mg-rich (Al). Therefore, HPT results in the formation of a phase structure which is closer to the equilibrium state than the initial coarse grained material.
3. The most probable mechanism of the equilibration of the (Al) supersaturated solid solution is the grain boundary diffusion accelerated by fluxes of vacancies produced due to SPD and by the sweeping of Mg and Zn atoms from the bulk by moving GBs.
4. Therefore, the SPD of supersaturated solid solutions can be considered as a balance between deformation-induced disordering and deformation-accelerated diffusion towards the equilibrium state.

Acknowledgements

The investigations were partly supported by the Deutsche Forschungsgemeinschaft, NATO Linkage grant (contract PST.CLG.979375), German Federal Ministry for Education and Research (contract RUS 04/014), INTAS (contract 03-51-3779) and Russian Foundation for Basic Research (RFBR contracts 03-02-16947, 03-02-0400, 04-03-32800). Fruitful discussions with Prof. W. Gust, Prof. M. Myshlyaev, Dr. E. Bischoff and Dr. W. Sigle are acknowledged.

References

- [1] Gleiter H. *Acta Mater* 2000;48:1.
- [2] Valiev RZ, Korznikov AV, Mulyukov RR. *Mater Sci Eng A* 1993;168:141.
- [3] Valiev RZ. *Ann Chim Fr* 1996;21:369.
- [4] Valiev RZ, Islamgaliev RK, Alexandrov IV. *Progr Mater Sci* 2000;45:103.
- [5] Nazarov AA, Romanov AE, Valiev RZ. *Acta Metall Mater* 1993;41:1033.
- [6] Senkov ON, Froes FH, Stolyarov VV, Valiev RZ. *Nanostruct Mater* 1998;10:691.
- [7] Likhachev VA, Rybin VV. *Izvestia AN SSSR Ser Fiz* 1973;37:2433 [in Russian].
- [8] Ivanisenko Yu, Lojkowski W, Valiev RZ, Fecht H-J. *Acta Mater* 2003;51:5555.
- [9] Rybin VV. *Large plastic deformation and fracture of metals*. Moscow: Metallurgia; 1986 [in Russian].
- [10] Rybin VV, Zisman AA, Zolotarevsky NYu. *Acta Metall Mater* 1993;41:2211.
- [11] Korznikov AV, Dimitrov O, Korznikova GF, Dallas J-P, Quivy A, Valiev RZ, et al. *NanoStruct Mater* 1999;11:17.
- [12] Nolfi Jr FV, editor. *Phase transformations during irradiation*. London, New York: Applied Science Publishers; 1983. p. 355.
- [13] Peterson NL, Rothman SJ. *Phys Rev B* 1970;1:3264.
- [14] Gödény I, Beke DL, Kedves FJ. *Phys Stat Sol (a)* 1972;13: K155.
- [15] Rothman SJ, Peterson NL, Nowicki LJ, Robinson LC. *Phys Stat Sol (b)* 1974;63:K29.
- [16] Ellwood EC. *J Inst Met* 1952;80:217.
- [17] Axon HJ, Hume-Rothery YW. *Proc Roy Soc* 1948;193:1.
- [18] Poole DM, Axon HJ. *J Inst Met* 1952;80:599.
- [19] Massalski TB et al., editors. *Binary alloy phase diagrams*. Materials Park (OH): ASM International; 1993. p. 3534.
- [20] Petzov G, Effenberg G, et al., editors. *Ternary alloys*, vol. 7. Weinheim: MSI-VCH; 1993. p. 497.
- [21] Kang Y-S, Araki H, Minamino Y, Yamane T, Saji S, Azuma K, et al. *J Jpn Inst Met* 1993;57:990.
- [22] Fujinaga Y, Sato TJ. *Alloys Compounds* 1994;209:311.
- [23] Zakharova MI, Ilina VA. *Zh Fiz Khim* 1950;24:714 [in Russian].
- [24] Martin G, Cauvin R, Barbu A. *Solid solution stability under irradiation*. In: Nolfi Jr FV, editor. *Phase transformations during irradiation*. London, New York: Applied Science Publishers; 1983. p. 47.
- [25] Chang L-S, Rabkin E, Straumal BB, Baretzky B, Gust W. *Acta Mater* 1999;47:4041.
- [26] Straumal B, Prokofjev SI, Chang L-S, Sluchanko NE, Baretzky B, Gust W, et al. *Def Diff Forum* 2001;188–190:1343.
- [27] Straumal BB, Zięba P, Gust W. *Int J Inorg Mater* 2001;3: 1113.
- [28] Rabkin EI, Semenov VN, Shvindlerman LS, Straumal BB. *Acta Metall Mater* 1991;39:627.
- [29] Rabkin EI, Shvindlerman LS, Straumal BB. *Int J Mod Phys B* 1991;5:2989.
- [30] Straumal BB. *Grain boundary phase transitions*. Moscow: Nauka publishers; 2003. p. 253 [in Russian].
- [31] Schölhammer J, Baretzky B, Gust W, Mittemeijer E, Straumal B. *Interf Sci* 2001;9:43.
- [32] Chang L-S, Rabkin E, Straumal BB, Hoffmann S, Baretzky B, Gust W. *Defect Diff Forum* 1998;156:135.
- [33] Noskovich OI, Rabkin EI, Semenov VN, Straumal BB, Shvindlerman LS. *Acta Metall Mater* 1991;39:3091.
- [34] Straumal BB, Noskovich OI, Semenov VN, Shvindlerman LS, Gust W, Predel B. *Acta Metall Mater* 1992;40:795.
- [35] Straumal B, Rabkin E, Lojkowski W, Gust W, Shvindlerman LS. *Acta Mater* 1997;45:1931.
- [36] Straumal B, Baretzky B. *Diff Def Forum* 2003;216–217:53.
- [37] Straumal BB, Sluchanko NE, Gust W. *Def Diff Forum* 2001;188–190:185.
- [38] Straumal BB, López G, Mittemeijer EJ, Gust W, Zhilyaev AP. *Diff Def Forum* 2003;216–217:307.
- [39] Straumal B, Lopez G, Gust W, Mittemeijer E. In: Zehetbauer MJ, Valiev RZ, editors. *Nanomaterials by severe plastic deformation Fundamentals – Processing – Applications*. New York: Wiley-VCH Verlag GmbH; 2004. p. 643.
- [40] Higashi K, Nieh TG, Mabuchi M, Wadsworth J. *Scripta Metall Mater* 1995;32:1079.

- [41] Takayama Y, Tozawa T, Kato H. *Acta Mater* 1999;47:1263.
- [42] Baró MD, Kolobov YuR, Ovid'ko IA, Schaefer H-E, Straumal BB, Valiev RZ, et al. *Rev Adv Mater Sci* 2001;2:1.
- [43] Utyashev FZ, Enikeev FU, Latysh VV. *AnnChim Fr* 1996;21:379.
- [44] Valiev RZ, Ivanisenko YuV, Rauch EF, Baudalet B. *Acta Metall* 1996;44:4705.
- [45] Korznikov AV, Tram G, Dimitrov O, Korznikova GF, Idrisova SR, Pakiela Z. *Acta Mater* 2001;49:663.
- [46] Cullity BD. *Elements of X-ray diffraction*. 2nd ed. Boston: Addison-Wesley Publishing; 1967. p. 356.
- [47] Pal U, Saha S, Chaudhuri AK, Rao VV, Banerjee HD. *J Phys D: Appl Phys* 1989;22:965.
- [48] Ungár T, Gubicza J, Ribárik G, Borbély A. *J Appl Cryst* 2001;34:298.
- [49] Ribárik G, Ungár T, Gubicza J. *J Appl Cryst* 2001;34:669.
- [50] Axon HJ, Hume-Rothery YW. *Proc Roy Soc* 1948;193:1.
- [51] Poole DM, Axon HJ. *J Inst Met* 1952;80:599.
- [52] Williamson GK, Hall WH. *Acta Metall* 1953;1:22.
- [53] Ungár T, Borbely A. *Appl Phys Lett* 1996;69:3173.
- [54] Ungár T, Ott S, Sanders P, Borbely A, Weertman JR. *Acta Mater* 1998;46:3693.
- [55] Ungár T, Dragomir I, Révész AA, Borbély A. *J Appl Cryst* 1999;32:992.
- [56] Friedel J et al. *Dislocations*. Oxford: Pergamon Press; 1964.
- [57] Blewitt TH, Coltman RR, Redman JK. *J Appl Phys* 1954;28:651.
- [58] Winterberger M. *Acta Metall* 1959;7:549.
- [59] Saada G. *Acta Met* 1961;9:166.
- [60] Saada G. *Acta Met* 1961;9:965.
- [61] Saada G. *Acta Met* 1962;10:551.
- [62] Beke DL, Gödény I, Erdelyi G, Kedves FJ. *Phylos Mag A* 1987;56:659.
- [63] Beke DL, Gödény I, Kedves FJ. *Phylos Mag A* 1983;47:281.
- [64] Beke DL, Gödény I, Kedves FJ. *Trans Jpn Inst Met Suppl* 1986;27:649.
- [65] Aleshin AN, Aristov VYu, Bokstein BS, Shvindlerman LS. *Phys Stat Sol (a)* 1978;45:359.
- [66] Aleshin AN, Bokstein BS, Petelin AL, Shvindlerman LS. *Metallofizika* 1980;2:83.
- [67] Zieba P, Pawlowski A, Gust W. *Def Diff Forum* 2001;194:1759.
- [68] Häbner A. *Isotopenpraxis* 1969;5:143.
- [69] Häbner A. *Krist Tech* 1973;8:K1.
- [70] Häbner A. *Krist Tech* 1974;9:1371.
- [71] Fujita T, Hasegawa H, Horita Z, Langdon TG. *Def Diff Forum* 2001;194:1205.
- [72] Fujita T, Horita Z, Langdon TG. *Phil Mag A* 2002;A82:2249.
- [73] Fujita T, Horita Z, Langdon TG. *Mater Sci Forum* 2002;396:1061.
- [74] Vladimirov AB, Kaygorodov VN, Klotsman SM, Symbelov VD, Trachtenberg IS. *Phys Metal Metallogr* 1975;39(1):78.
- [75] Minamino Y, Toshimi Y, Shinomura A, Shimada M, Koizumi M, Ogawa N, et al. *J Mater Sci* 1983;18:2679.
- [76] Erdelyi G, Lojkowski W, Beke DL, Gödény I, Kedves FJ. *Phil Mag A* 1987;56:673.